Journal of Power Sources 195 (2010) 3394–3401

Contents lists available at ScienceDirect

Journal of Power Sources

journal homepage: www.elsevier.com/locate/jpowsour

Alloys and oxides on carbon-supported Pt–Sn electrocatalysts for ethanol oxidation

D.R.M. Godoi, J. Perez, H.M. Villullas*

Departamento de Físico-Química, Instituto de Química, Universidade Estadual Paulista – UNESP, Caixa Postal 355, R. Francisco Degni, s/n, CEP 14801-970, Araraquara, SP, Brazil

ARTICLE INFO

Article history:
Received 27 October 2009
Received in revised form 9 December 2009
Accepted 10 December 2009
Available online 21 December 2009

Keywords:
Ethanol oxidation
Electrocatalyst
Pt-based nanoparticles
Nanostructured materials

ABSTRACT

This work reports studies of ethanol oxidation on Pt–Sn/C catalysts with nearly the same particle size and identical overall composition having different amounts of oxide and alloyed phases. Results of characterization of physical properties by transmission electron microscopy (TEM), X-ray diffraction (XRD), differential scanning calorimetry (DSC), X-ray photoelectron spectroscopy (XPS), and in situ dispersive X-ray absorption spectroscopy (DXAS) are presented. The variation in the amount of oxide and alloyed phases, promoted by heat treatments in mild temperature conditions, does not produce any significant particle growth. Cyclic voltammetry and oxidation of adsorbed CO in acid medium are used to probe the surface conditions. Data on the electrocatalytic activity towards ethanol oxidation, obtained by potential sweeps and chronoamperometry, are discussed and correlate well with the physical properties. This study, carried out in the absence of composition and particle size effects, shows that the electrocatalytic activity towards ethanol oxidation is strongly influenced by the changes in the amounts of Sn in alloyed and oxidized forms, and that the increase in the amount of alloy at expense of the oxides improves the catalytic activity.

1. Introduction

In spite of the progress that resulted from research concerning the most different aspects of fuel cell technology, it is not possible yet to produce electric power with acceptable efficiency using ethanol in proton exchange membrane fuel cells (PEMFC). The use of ethanol in direct alcohol fuel cells (DAFC) is extremely interesting because it can be obtained from biomass, as is the case of the Brazilian sugarcane ethanol. Ethanol also has high power density and rather low toxicity.

Pt is not the best catalyst for the electrochemical oxidation of small organic molecules, such short chain alcohols. The electrochemical oxidation of ethanol on pure Pt produces strongly adsorbed poisoning intermediates, such as CO, and generates undesirable products through parallel reactions, such as acetic acid and acetaldehyde, causing a considerable loss of ability for generating electricity. The cleavage of the C–C bond of the ethanol molecule needed for its complete oxidation to CO_2 has remained one of the major challenges in ethanol oxidation electrocatalysis [1,2]. Therefore, a desirable catalyst must be able to activate C–C bond breaking, avoiding the poisoning of the active sites by the residues of the reaction, and thus decreasing the amounts of the partial oxidation products.

The most common approach to enhancing activity for the electrochemical oxidation of alcohols, such as methanol and ethanol, has been the development of binary and/or ternary alloys with Pt using alloying metals that could help to mitigate the poisoning effects seen on Pt [3]. So far, Pt–Ru and Pt–Sn are the most active materials for methanol and ethanol oxidation, respectively. The enhancement of the catalysis of alcohol oxidation on these materials is generally interpreted in terms of the ability of the second metal to supply, in lower potentials, the hydroxyl species necessary for the complete oxidation of the alcohol and for the removal of the CO formed in the intermediate reaction steps that poisons the catalyst surface [4–7]. The enhanced activity for the oxidation of methanol of Pt particles dispersed on oxide matrixes has also been interpreted on these bases [8,9]. On the other hand, electronic effects have also been attributed to the second metal, which would result in weakening the bond between the adsorbed CO and the catalyst surface [4,6,10,11]. Recent work on Pt–Ru/C catalysts has shown that not only the second metal but also the oxides influence the occupancy of the Pt 5d band [12].

In general, the currents of ethanol oxidation are larger on Pt–Sn/C catalysts than on Pt/C, and the reaction has lower onset potentials. Despite the fact that CO_2 yields lower than for Pt were reported for Pt–Sn/C catalysts, indicating that are not effective for the C–C bond breaking [13], Pt–Sn catalysts are still considered the

* Corresponding author. Tel.: +55 16 33016653; fax: +55 16 33016692.
E-mail address: mercedes@iq.unesp.br (H.M. Villullas).

0378-7753/$ – see front matter © 2009 Elsevier B.V. All rights reserved.
doi:10.1016/j.jpowsour.2009.12.037

most active materials for ethanol oxidation. The electrochemical oxidation of ethanol has been extensively studied on Pt–Sn catalysts of different compositions, which were prepared by a variety of methods, such as carbon co-impregnation followed by reduction [14–23], the Bonneman's method [1], and in microemulsions [24], just to mention a few. Analysis of those catalysts usually showed that most of the Sn was not alloyed but in oxidized states. In addition, significant ethanol oxidation current enhancement has been reported for $PtSnO_x$ systems [25,26], and interpreted on the basis of a bifunctional mechanism, i.e., the OH species supplied by tin oxide would facilitate the removal of CO-like species and ethanolic residues.

In spite of the large number of published studies on the oxidation of ethanol on Pt–Sn/C materials, to analyze the role that alloyed phases and oxides play in the current enhancement is not an easy task. Comparison of literature results is rather difficult because of the different physical properties of the catalysts used in each study. In general terms, a large amount of data on Pt-based binary materials prepared by a variety of methods evidence that the catalysts properties, such as composition, structure, morphology, particle size, and degree of alloying, are strongly dependent on synthesis conditions. Thus, it is not surprising to find significant differences in the electrocatalytic activities of Pt–Sn/C materials reported in the literature, as they seem to depend on the preparation methodology adopted in each case. A detailed understanding of the role of alloyed and oxide phases as well as the elucidation of the mechanistic aspects of ethanol oxidation on carbon-supported Pt–Sn catalysts seems crucial to improve the electrocatalysis of ethanol oxidation and for developing new and more efficient materials.

In this work, ethanol oxidation was studied on Pt–Sn/C catalysts heat-treated under different atmospheres that promoted changes in the amount of oxides and degree of alloying aiming to evaluate the effects of alloyed and oxide phases on the measured currents. Particle growth was avoided by carrying out the heat treatments under mild temperature conditions. Thus, carbon-supported Pt–Sn materials with nearly identical particle size and particle distributions were obtained. Considerable differences in electrocatalytic activities toward ethanol and adsorbed CO oxidation were observed on these Pt–Sn/C catalysts, which are discussed here in terms of surface composition (oxide and alloy), for materials having exactly the same overall composition, and in the absence of particle size effects.

2. Experimental

2.1. Catalysts preparation

Pt–Sn/C catalysts were obtained by a procedure similar to that described elsewhere [12,27]. Briefly, in order to avoid the influence of the carbon support on particle growth the Pt–Sn nanoparticles were first obtained in a colloidal state using a water/n-heptane/AOT microemulsion as synthesis medium. Thus, an aqueous solution of H_2PtCl_6 and $SnCl_2$ (0.5 wt% metals and 7:3 Pt:Sn atomic ratio) was added to a mixture of n-heptane and AOT (15 wt%) under constant stirring. The amount of aqueous solution of the precursors that was added produced a microemulsion with water to surfactant molar ratio (w) equal to 8. Pt–Sn nanoparticles were formed by reduction of the precursors with $NaBH_4$, which was added to the microemulsion as a solid in a molar ratio of 10:1 to metals. The resulting mixture was kept under constant stirring for 2 h and then an appropriate amount of high surface area carbon (Vulcan XC-72, Cabot) was added in order to obtain the supported catalysts. The suspension was then stirred for 15 h. All materials were 20% (w/w) metal (Pt + Sn) on carbon. The supported catalysts thus formed were filtered, washed copiously with ethanol, acetone, and ultra-pure water and dried at 80 °C for 1 h. All reagents were purchased from Aldrich and used without further purification.

To modify the catalysts surface without producing significant changes in the average particle size, the as-prepared sample was divided into three parts and two of them were heat-treated in mild temperature conditions (150 °C, 1 h). In this way, the as-prepared and heat-treated Pt–Sn/C catalysts had exactly the same overall composition. One sample was treated in nitrogen and the other one in a pure hydrogen atmosphere.

2.2. Catalysts characterization

The Pt–Sn/C catalysts were examined by X-ray diffraction (XRD) using a Rigaku, model D Max 2500 PC diffractometer. The X-ray diffractograms were obtained with a scan rate of $1^\circ\,min^{-1}$ and an incident wavelength of 0.15406 nm (Cu Kα). A Philips CM200 instrument operating at 200 kV was used for the transmission electron microscopy (TEM) study. Differential scanning calorimetry (DSC) measurements were performed using a TA Instruments differential scanning calorimeter model DSC Q-20, under nitrogen flux of 50 mL min^{-1}, and with a scan rate of 5 °C min^{-1}.

X-ray photoelectron spectroscopy (XPS) studies were carried out using a commercial spectrometer (UNI-SPECS UHV). The Mg Kα line was used ($h\nu$ = 1253.6 eV) and the analyzer pass energy was set to 10 eV. The inelastic background of the Pt 4f and Sn 3d electron core-level spectra was subtracted by using Shirley's method. The composition of the surface layer was determined from the ratio of the relative peak areas corrected by sensitivity factors of the corresponding elements. The spectra were fitted without placing constraints using multiple Voigt profiles. The width at half maximum (FWHM) varied between 1.6 and 2.0 eV and the accuracy of the peak positions was ±0.1 eV.

In situ dispersive X-ray absorption spectroscopy (DXAS) experiments were performed for all samples at the DXAS beam line of the Brazilian Synchrotron Light Laboratory (LNLS), Brazil [28]. The measurements were carried out in a spectroelectrochemical cell [29], using catalysts as pellets prepared by pressing a mixture of a Nafion® solution and the catalyst powder (Pt load was 6 mg cm^{-2}). Measurements were done at constant applied potentials of 0.4, 0.6, 0.8 and 1.0 V vs. RHE, in 0.5 mol L^{-1} H_2SO_4 solutions. An X-ray beam with a bandwidth of a few hundred eV around the Pt L_3 edge (11,564.25 eV) was selected using a curved Si(111) crystal monochromator. Its bending mechanism focused the beam at the sample position and the transmitted beam was collected by using a CCD camera. The exposure time was set for 150 ms for each measured spectrum. In order to improve the signal-to-noise ratio, 100 accumulations (frames) compose a full spectrum with 1.5 s of total acquisition time. Conversion of data, pixel to energy, was performed by comparing measurements in conventional mode with those in dispersive mode from standard foils (Pt metal).

2.3. Electrochemical measurements

The general electrochemical behavior was characterized by cyclic voltammetry in 0.5 mol L^{-1} H_2SO_4, and the electrocatalytic activity towards ethanol oxidation was evaluated in 0.5 mol L^{-1} ethanol acid solution by linear sweep voltammetry and chronoamperometry. All experiments were done at 25 °C in Ar saturated solutions. CO stripping experiments were carried out in the following way: after recording a cyclic voltammetry curve in an Ar purged system, CO was admitted to the cell and adsorbed at 0.15 V vs. RHE for 20 min. The adsorption potential was chosen considering that the pre-oxidation wave is observed only if CO is adsorbed in the 0.0–0.15 V potential range [30], and that OH adsorption on Sn might start taking place around 0.28 V [31]. The excess CO was

Table 1
TEM results for the Pt–Sn/C catalysts prepared.

Pt–Sn/C catalyst	TEM particle size/nm	σ
As-prepared	3.0	0.19
Treated in N_2	3.0	0.18
Treated in H_2	3.2	0.20

eliminated by passing Ar gas during 30 min and the adsorbed CO was oxidized at a scan rate of 5 mV s^{-1}.

All electrochemical measurements were done in a conventional electrochemical cell, with a Pt wire counter-electrode placed in a separate compartment and a reversible hydrogen reference electrode. The Pt–Sn/C electrocatalysts were used as ultra-thin layers [32] on a glassy carbon disk electrode (0.196 cm^2) previously polished down to 0.3 μm alumina. In all cases, the catalysts layers had a metal (Pt + Sn) load of 28 μg cm^{-2}. A Pt/C sample prepared in the same microemulsion system was used to assess the effectiveness of the cleaning procedure and a Pt/C commercial catalyst (E-TEK) was used as reference sample. Because electrodes contained the same amount of noble metal, currents densities were calculated for the geometric area of the glassy carbon disk. Solutions were prepared from analytical grade H_2SO_4 (Mallinckrodt), analytical grade ethanol (J. T. Baker) and ultra-pure water (MilliQ, Millipore).

3. Results and discussion

3.1. Physical characterization

Typical TEM images of the Pt–Sn/C catalysts, taken with low magnification to give a general view of the materials, are shown in Fig. 1. It can be observed that for all samples, particles were uniformly dispersed on the carbon support, with the presence of few aggregates. Particle size distribution histograms obtained from TEM studies are shown in Fig. 2. The average particle size was calculated by the mean value of the Gaussian curve adjusted to the distribution histogram. The results show that all samples have similar mean particle sizes providing evidence that heat treatment at 150 °C did not produce significant particle growth. In a general way, the heat treatment in mild temperature conditions did not cause any significant broadening of the particle size distribution histograms and the polydispersity index (σ = standard deviation/mean value) remained nearly the same. TEM results are summarized in Table 1.

Slightly larger values of average particle size and polydispersity were obtained for the Pt/C sample (3.6 nm and σ = 0.16). While particle size for the 20% Pt/C commercial catalyst used as control was not determined in this study, particle sizes between 2.5 and 4.0 nm [33] and of 3.4 ± 1.2 nm [34] have been previously reported.

X-ray diffraction analysis showed diffraction patterns associated to the Pt fcc structure (JCPDS 4–802) for all three Pt–Sn/C samples, as shown in Fig. 3. Diffraction signals for the as-prepared and nitrogen-treated Pt–Sn/C catalysts appear, in general, at 2θ values nearly identical to those measured for Pt/C, for which the lattice constant was 3.908 Å. In contrast, diffraction peaks show a pronounced shift to lower 2θ values for the hydrogen-treated catalyst. This shift in peak position can be taken as evidence of alloy formation because of partial substitution of Pt by Sn in the fcc structure which produces an expansion of the lattice (lattice parameter 3.939 Å). It is also observed that diffraction peaks of as-prepared samples are broader than for heat-treated catalysts, as shown in the inset of Fig. 3 for the [2 2 0] reflections. The mean crystallite sizes estimated using Scherrer's equation were 2.2 nm for the as-prepared sample and 2.8 nm for both heat-treated catalysts.

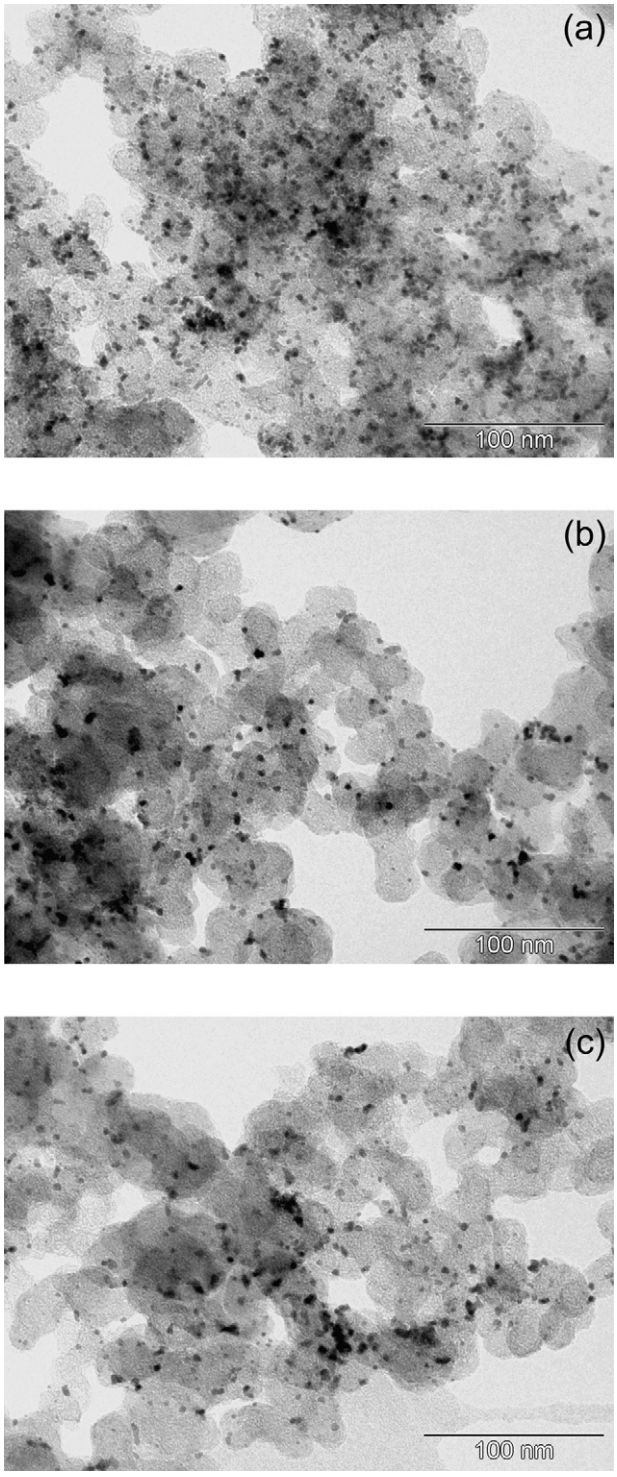

Fig. 1. TEM micrographs for the Pt–Sn/C catalysts. (a) As-prepared; (b) heat-treated in nitrogen; (c) heat-treated in hydrogen.

Small diffraction signals that could be attributed to SnO_2 (41-1445) were apparent at 2θ values around 33° and 51°. Therefore, the presence of tin also in the form of amorphous oxides cannot be discarded. A detailed XRD analysis for these species could not be performed because of the low intensity of the signals and the interference of the signals from Pt and the carbon support.

Differential scanning calorimetry (DSC) can be used to investigate the restructuring processes that this type of materials undergo

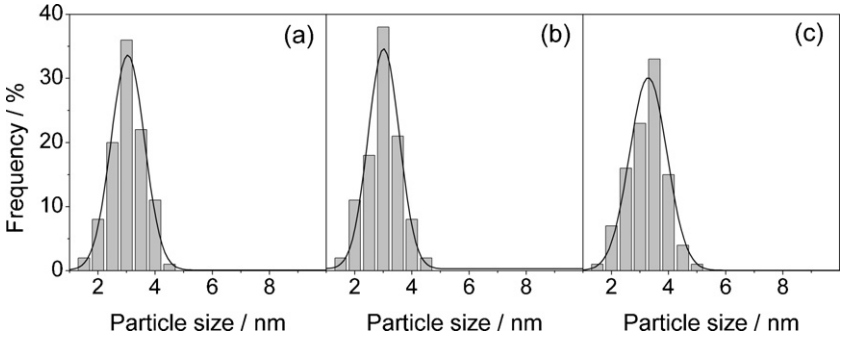

Fig. 2. Particle size distributions obtained from TEM images for the Pt–Sn/C catalysts. (a) As-prepared; (b) heat-treated in nitrogen; (c) heat-treated in hydrogen.

when heated. Godoi et al. [27] showed that carbon-supported Pt nanoparticles prepared in AOT/n-heptane/water microemulsions show a well defined exothermic event at around 150 °C, which could be associated to a restructuring process with an increased in the crystallinity. Fig. 4 shows the DSC curve obtained in N_2 atmosphere for the as-prepared Pt–Sn/C catalyst. An endothermic event occurs between ambient temperature and 100 °C, followed by an irreversible exothermic transition, which ends at around 150 °C, very similar to that observed for Pt/C materials. Besides the evidence regarding the fact that the Pt–Sn/C material also goes through a crystallization process, that is also evident by the increase in the average crystallite size calculated from XRD data, the peak associated to the exothermic event appears to be broadened when compared to the one observed for pure Pt supported on carbon. DSC curves of substances containing an impurity generally show broader crystalline transition peaks than the pure compounds [35]. Because the incorporation of a small amount of a second metal into the Pt crystalline structure would have an effect similar to that of an impurity, the observed broadening of the crystalline transition peak can be taken as evidence of the existence of an alloyed phase in the as-prepared Pt–Sn/C sample. Because the presence of an alloyed phase was not apparent in the X-ray diffraction pattern of the as-prepared catalyst, it can be inferred that the amount of Sn alloyed with Pt in the as-prepared Pt–Sn/C catalysts is rather small.

X-ray photoelectron spectroscopy analysis. XPS studies were carried out for all three Pt–Sn/C catalysts. For the sake of simplicity, the as-prepared Pt–Sn/C catalyst was chosen as reference sample. The Pt 4f and Sn $3d_{5/2}$ high-resolution XPS spectra are shown in Fig. 5.

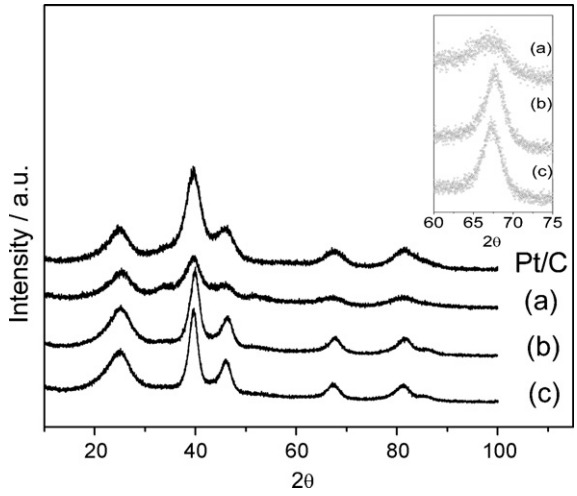

Fig. 3. X-ray diffraction patterns for the Pt–Sn/C catalysts. (a) As-prepared; (b) heat-treated in nitrogen; (c) heat-treated in hydrogen. Results for a Pt/C commercial catalyst (E-TEK) are included for comparison. Inset: enlarged view of the [2 2 0] diffraction peaks of the Pt–Sn/C catalysts.

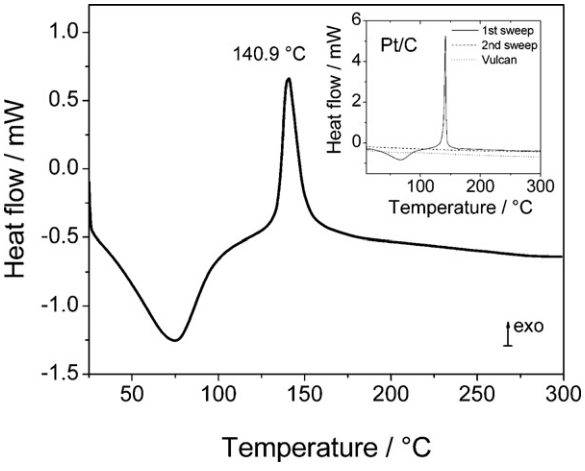

Fig. 4. DSC curve in nitrogen atmosphere for the as-prepared Pt–Sn/C catalyst. Inset: DSC curves for a Pt/C catalyst prepared by the same method and for the Vulcan XC-72 carbon support.

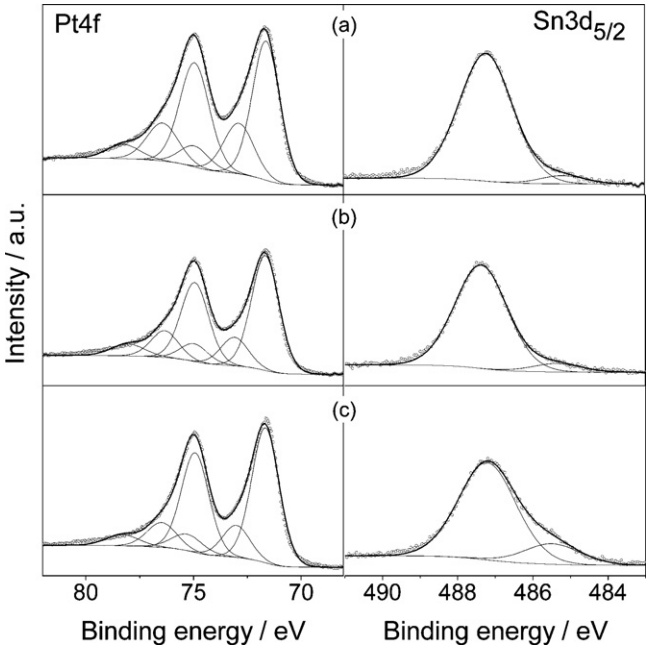

Fig. 5. Pt 4f and Sn $3d_{5/2}$ XPS spectra for the Pt–Sn/C catalysts. (a) As-prepared; (b) heat-treated in nitrogen; (c) heat-treated in hydrogen.

Table 2
Binding energies of the Pt $4f_{7/2}$ components for the Pt–Sn/C catalysts and atomic percentage for each signal.

Pt–Sn/C catalysts			Assignment [36]
As-prepared	Treated in N_2	Treated in H_2	
71.64 (64.5)	71.67 (68.8)	71.67 (72.1)	Pt(0)
72.90 (25.4)	73.10 (19.7)	73.02 (18.0)	$Pt(II)–Pt(OH)_2$
74.96 (10.1)	74.97 (11.5)	75.30 (9.8)	$Pt(IV)–PtO_2$; $PtO_2 \cdot nH_2O$

Table 3
Binding energies of the Sn $3d_{5/2}$ components for the Pt–Sn/C catalysts and atomic percentage for each signal.

Pt–Sn/C catalysts			Assignment [40]
As-prepared	Treated in N_2	Treated in H_2	
485.18 (5.2)	485.37 (7.1)	485.49 (17.0)	Sn(0)
487.21 (94.8)	487.38 (92.9)	487.21 (83.0)	$Sn(IV)–SnO_2$

The Pt 4f spectrum was deconvoluted into three doublets which correspond to Pt $4f_{7/2}$ and Pt $4f_{5/2}$ of different oxidation states. The line with major intensity centered at around 71.7 eV can be assigned to Pt in the zero-valence metallic state, shifted toward higher values with respect to the literature value of 71.2 eV [36]. A slight shift of the Pt(0) peak to higher binding energies is a known effect for small particles [37]. Also, peak shifts toward higher values of binding energies for the Pt $4f_{7/2}$ in relation to pure Pt have been reported for carbon-supported [38] and zeolite-supported Pt [39], as well as for Pt nanoparticles dispersed on RuO_2 matrixes [8,9], and they have been interpreted as caused by Pt-support interactions. The binding energies of the Pt $4f_{7/2}$ components centered at 72.9–73.0 eV and 74.9–75.3 eV can be attributed to Pt(II) and Pt(IV) species [36]. The binding energies obtained for the components of the Pt $4f_{7/2}$ peak are shown in Table 2 together with the atomic percentage for each signal.

In general, Pt is found in the zero-valence state and in ionic form, most likely as $Pt(OH)_2$ and PtO_2. The data evidence that heat treatments at 150 °C in nitrogen and hydrogen produced an increase in the amount of metallic Pt while the quantity of hydrated oxides decreased.

The Sn $3d_{5/2}$ signal was deconvoluted into two different peaks. The first line centered at 485.1–485.5 eV can be attributed to Sn in the zero-valence state while the second line (487.1–467.4) can be assigned to Sn(IV) species [40]. As it can be seen, the amount of Sn in the zero-valence metallic state for the Pt–Sn/C catalyst treated in nitrogen is similar to that in the as-prepared catalyst, and significantly larger for the hydrogen-treated material. Table 3 shows the binding energies and the atomic percentage for each signal.

Overall, XPS data revealed that heat treatments in nitrogen and hydrogen produced an increase in the amount of metallic Pt in both Pt–Sn/C catalysts. Additionally, the amounts of metallic Sn and Sn oxides remained nearly the same for the material heat-treated in nitrogen while there was a substantial increase in the content of metallic Sn (with concomitant decrease in the content of Sn oxides) for the catalyst treated in hydrogen.

3.2. Dispersive X-ray absorption spectroscopy

In situ DXAS measurements were done to probe the electronic characteristics of Pt–Sn/C catalysts. The analysis of white lines was performed by using the method of Shukla et al. [41,42]. The absorption spectra were fitted by an arc tangent function which was subtracted from the experimental data, and the result was fitted by a Lorentzian function. The Levenberg–Marquardt nonlinear regression method [43] was used in both fitting procedures.

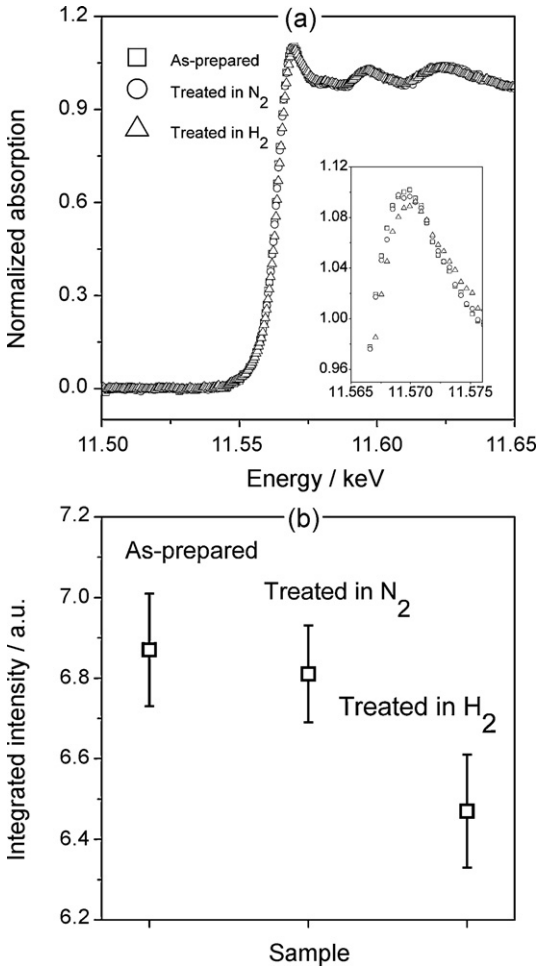

Fig. 6. (a) Normalized Pt L_3 absorption for different samples. (b) Integrated intensities of the Lorentzian. Applied potential: 0.80 V.

In general, all samples showed an increase of the normalized absorption intensity (white line) intensity and integrated intensity of the Lorentzian for increasing applied potential, resulting from the adsorption of oxygenated species, in agreement with literature reports [44,45]. Furthermore, at any applied potential the integrated intensity of the Lorentzian followed the same trend, decreasing significantly for the hydrogen-treated catalyst (around 7–10% depending on potential). Fig. 6 shows the normalized Pt L_3 absorption edges and the integrated intensities of the Lorentzian for the different Pt–Sn/C catalysts polarized at 0.80 V.

Mukerjee and McBreen [46] reported a lowering of the white line intensity for a Pt–Sn/C commercial alloy catalyst (E-TEK, Pt:Sn atomic composition 3:1) as compared to the Pt foil, which was interpreted as a filling of the Pt 5d bands resulting of alloying with Sn. In good agreement with that, for all Pt–Sn/C catalysts prepared in this work the normalized absorption intensity was lower than for Pt/C. To interpret the DXAS results of Fig. 6 it should be kept in mind that a decrease in the amount of oxygenated species will also lead to a decrease of the white line intensity. Therefore, the decrease in the white line intensity observed for the Pt–Sn/C catalysts heat-treated in hydrogen is consistent with an increase in the degree of alloying, as evidenced by XRD data and the concomitant decrease in the amount of oxidized species in good agreement with XPS data.

The fact that the white line intensity observed for the Pt–Sn/C catalyst heat-treated in nitrogen is similar to that of the as-prepared material is also in good agreement with XRD and XPS results that

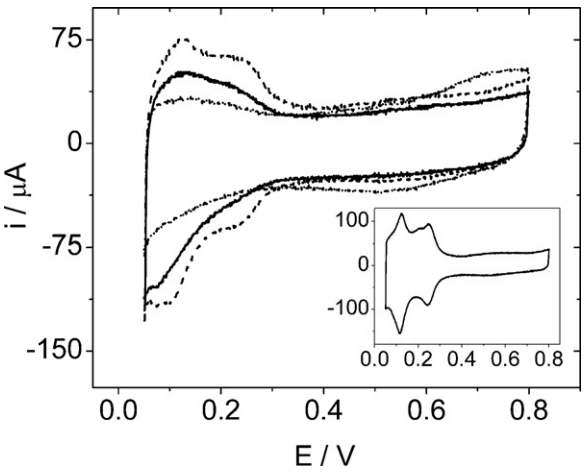

Fig. 7. Current–potential curves of the Pt–Sn/C catalysts obtained in H_2SO_4 0.5 mol L^{-1} at 50 mV s^{-1}. (—) As-prepared; (– – –) treated in N_2; (–···–) treated in H_2. The curve of the Pt/C catalyst prepared by the same method is shown in the inset for comparison.

show that the amounts of metallic Sn and Sn oxides in those two samples are comparable.

3.3. Electrochemical behavior and electrocatalysis of ethanol oxidation

The electrochemical properties of the Pt–Sn/C catalysts were first examined by cyclic voltammetry. The curves obtained at 50 mV s^{-1} in Ar saturated 0.5 mol L^{-1} H_2SO_4, in the potential range of 0.05–0.8 V, are shown in Fig. 7. The curve obtained for the Pt/C prepared by the same microemulsion method (inset) serves as evidence that the washing procedure adopted for removal of synthesis residues was efficient and produced clean particles. For all Pt–Sn/C samples, the general features of the voltammetric curves are similar to those typical of Pt-based catalysts supported on carbon while differences in the total charges involved in the current–potential curves are apparent. The state of the surface can be qualitatively assessed by the analysis of the hydrogen adsorption–desorption region. While it is known that adsorption of underpotential deposited hydrogen does not take place on Sn [47,48] or SnO_2 [49], quantitative evaluation of the Pt surface area is not possible because, as mentioned before, OH adsorption on Sn might start taking place around 0.28 V [31]. Comparison of the voltammetric curves, however, reveals that heat treatment in nitrogen produced an increase in the charge in the hydrogen adsorption–desorption region. In addition, the features characteristic of the hydrogen adsorption–desorption processes on polycrystalline Pt surfaces appear better defined. The current-potential profile becomes more Pt-like, which could result from Pt surface enrichment or segregation caused by the heat treatment. In contrast, the curve of the Pt–Sn/C catalyst heat-treated in hydrogen shows a significantly smaller hydrogen adsorption–desorption, which can be ascribed to an increase in the metallic Sn content of the surface due to alloy formation resulting in a decrease in the amount of Pt on the surface.

While it is widely accepted that Pt–Ru/C and Pt–Sn/C are less poisoned by strongly adsorbed intermediates (CO) from the dissociation of alcohols than Pt/C [55], a recent study has shown that the Pt–Ru/C catalyst that produced the largest currents of methanol oxidation was not the most efficient for the oxidation of adsorbed CO [12].

The curves of adsorbed CO oxidation recorded at 5 mV s^{-1} on the three Pt–Sn/C catalysts prepared in this work are shown in Fig. 8. The peak potential was significantly lower for all Pt–Sn/C samples than for the Pt/C commercial catalyst (0.77 V). The oxidation of adsorbed CO shows a well defined current peak centered at about 0.70 V for the as-prepared catalyst and at around 0.68 V for the Pt–Sn/C material treated in hydrogen. In contrast, the curve for the sample treated in nitrogen shows two superimposed oxidation peaks, at around 0.68 and 0.74 V. The presence of the second signal is very close to that observed for the pure Pt commercial catalyst and consistent with the more Pt-like surface evidenced by the cyclic voltammetry curves of Fig. 7, indicating that the absence of a reducing atmosphere during treatment favors Pt segregation on the catalyst surface. According to the bifunctional mechanism, Sn would act as donor of the OH species which would promote the oxidative removal of CO-like species from the surface at lower potentials. On the other hand, as evidenced by the DXAS data for the Pt L_3 absorption edge (Fig. 6), increasing the amount of metallic Sn resulted in a decrease in the white line intensity. Thus, this electronic effect that might promote the weakening of the bond between CO and the catalyst surface, as suggested in the literature [4,6,10,11].

The validity of the determination of the active surface area of the catalysts from the charge of oxidation of adsorbed CO is a controversial matter. Weaver et al. [50] pointed out the necessity of charge correction for anion adsorption and double layer charging. Unfortunately, there is no consensus at present about how this should be done.

However, when active surface areas were estimated without making any corrections besides subtracting the currents in the cyclic voltammetry in the base electrolyte, similar values (around 27 m^2 $g_{Pt}{}^{-1}$) were obtained for all Pt–Sn/C prepared in this work, in good agreement with literature [20].

Fig. 9 shows the linear sweep voltammetry curves of ethanol oxidation. As expected, the onset potentials of the ethanol oxidation reaction are lower (0.25 V) for the Pt–Sn/C catalysts compared to the commercial Pt/C catalyst (0.35 V). Fig. 10 shows the

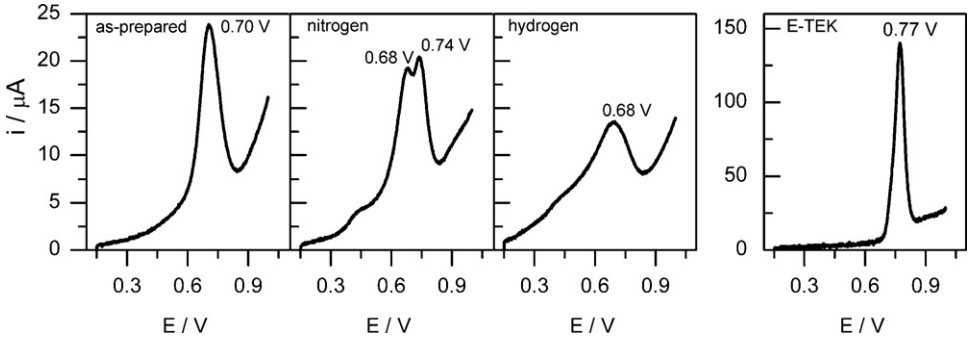

Fig. 8. Current–potential curves of oxidation of adsorbed CO for the as-prepared and heat-treated Pt–Sn/C catalysts, as indicated. The curve for the Pt/C commercial catalyst (E-TEK) is included for comparison. Sweep rate: 5 mV s^{-1}.

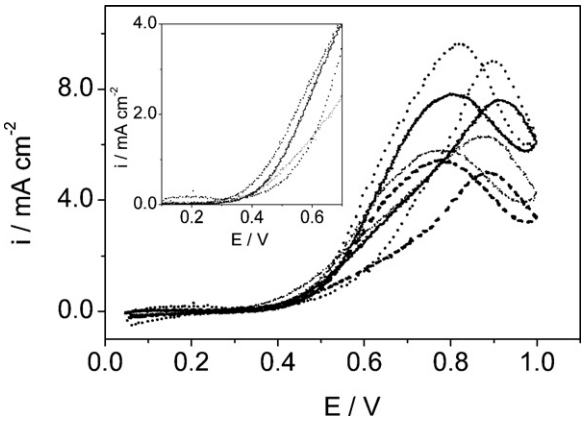

Fig. 9. Current density–potential curves obtained at 20 mV s^{-1} in H_2SO_4 0.5 mol L^{-1} + ethanol 0.5 mol L^{-1} for the Pt–Sn/C catalysts. (—) As-prepared; (– – –) treated in N_2; (–·–) treated in H_2; (···) Pt/C commercial catalyst (E-TEK). The initial portions of the positive sweeps are shown in the inset.

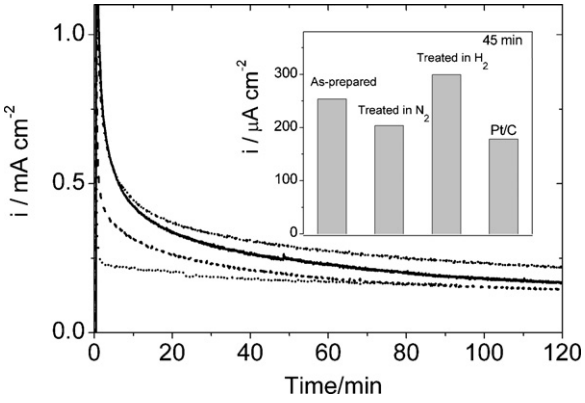

Fig. 10. Current density–time curves for ethanol oxidation obtained at 0.5 V for Pt–Sn/C catalysts. (—) As-prepared; (– – –) treated in N_2; (–·–) treated in H_2; and (···) Pt/C commercial catalyst (E-TEK). Inset: current densities measured at 45 min. Electrolyte: 0.5 mol L^{-1} ethanol + 0.5 mol L^{-1} H_2SO_4.

current–time curves recorded at 0.5 V, which in general terms exhibit the same tendency observed for the linear sweep study. The current–time curve for the catalyst heat-treated in nitrogen presented the lowest current while the highest currents were measured for the Pt–Sn/C catalyst heat-treated in hydrogen. It is also interesting to note that ethanol oxidation and the oxidation of adsorbed CO follow the same trend, in contrast with recent findings for Pt–Ru/C catalysts [12].

As already mentioned, the significant differences in the electrocatalytic activities of Pt–Sn/C materials reported in the literature seem to depend on the preparation procedure adopted. Recent studies on Pt–Ru/C catalysts showed that the amounts of oxide and alloyed phases are size dependent [27], which might also be the case for other Pt-based materials such as Pt–Sn and thus, the reasons for the different results on electrocatalytic activity reported in the literature may rest not just on the different compositions and particle sizes of the materials studied but also on the different ratios of alloy to oxides. While some attempts to assess the relative contributions of Pt–Sn alloys and SnO_2 to the enhancement of ethanol oxidation have been made, comparison of results obtained for catalysts prepared by different methods and having quite different properties did not lead to any agreement on that matter. The enhanced activity of Pt–SnO_2/C was interpreted by Mann et al. [52] as evidence that a platinum–tin alloy is not a necessary catalytic phase for ethanol oxidation. In contrast, studies carried out by Colmati et al. [20] found that the activity of Pt–Sn/C catalysts seems to depend on the amount of both nonalloyed and alloyed tin. Based on those observations, the existence of an optimal distribution of Sn between the alloyed and nonalloyed states was suggested [20]. Zhu et al. [53] prepared Pt–SnO_2/C and carbon-supported Pt–Sn catalysts using different synthesis procedures to vary the degree of alloying and concluded that low alloying degree would enhance the yield of acetic acid while Pt–Sn/C catalyst with high alloying degree promote the entire activity for ethanol oxidation.

It is important to stress that the present study of the effects of the amounts of oxide and alloy phases was carried out on Pt–Sn/C catalysts having nearly the same particle size and exactly the same overall composition. The voltammetry curves (Fig. 7) as well as the data of CO stripping (Fig. 8) suggest that the heat treatment in nitrogen caused Pt segregation and, therefore, the smaller catalytic activity for ethanol oxidation can be understood as resulting from a more Pt-like surface. Yet, comparison of the results of ethanol oxidation obtained for the as-prepared Pt–Sn/C catalysts with those obtained for the pure Pt/C commercial sample reveals clearly that the presence of Sn, even if mostly in a nonalloyed (oxidized) state, has an enhancement effect. These observations that indicate that the presence of oxidized Sn species benefits the ethanol oxidation reaction are in agreement with previous literature reports [20] and with the enhanced activity exhibited by Pt–SnO_2/C materials [51,52]. According to the DRX data, the heat treatment in hydrogen atmosphere promoted an increase in the alloying, which enhanced the catalytic activity for ethanol oxidation in agreement with data formerly reported [1,21,54–56]. It is also noteworthy that the current densities of ethanol oxidation shown in Fig. 10 follow the same trend that the integrated intensity of the Pt L_3 adsorption edge (Fig. 6b), indicating that the activity improvement produced by the increase in the amount of alloy is also linked to the occupancy of the Pt d band. While increasing the amount of alloy results in a reduced white line intensity, which has been interpreted in terms of the lesser vacancy of the Pt 5d band [46], it is known that oxygenated species produce a lesser occupancy of the Pt d band, leading to an increase of the normalized absorption intensity (white line).

In summary, the present study was made in the absence of overall composition and particle size effects. The results reported here evidence that even though the presence of Sn oxide species might be sufficient to produce higher currents than those measured on Pt/C, increasing the amount of metallic Sn at the expense of the oxides, which lead to a more filled Pt d band, results in an increase of the activity of Pt–Sn/C catalysts for ethanol oxidation.

While the data presented herein show that increasing the amount of alloy results in larger ethanol oxidation currents, detailed analysis of the product distribution is necessary to further understand the role of oxides and alloys in the electrocatalysis of ethanol oxidation on Pt–Sn/C materials and to elucidate their effects on the reaction mechanism. Studies of that kind are currently under way in our laboratory.

4. Conclusions

Pt–Sn/C catalysts with a narrow particle size distribution and a uniform distribution on the carbon support were prepared by using a microemulsion method. To modify the amounts of oxide and alloyed phases, portions of the as-prepared catalyst were treated in different atmospheres and therefore, all Pt–Sn/C catalysts studied had exactly the same overall composition. Because particle growth was avoided by using mild temperature conditions, the materials also had nearly the same particle size.

While it was verified that the presence of oxidized Sn has an enhancement effect, mild heat treatment in hydrogen atmosphere produced an increase in the amount of alloy and an enhancement of the ethanol oxidation current. That enhancement can be explained

in terms of a more filled Pt 5d band when the amount of alloy increases. The oxidation of adsorbed CO follows the same trend.

In summary, the present study was made in the absence of overall composition and particle size effects and showed that even though Pt–Sn/C materials have good catalytic activity for the oxidation of ethanol when Sn is mostly in a nonalloyed state, the oxidation current can be enhanced by the increase of the amount of alloyed phase at expense of the oxides.

Acknowledgments

Thanks are due to the Brazilian Agencies Fundação de Amparo à Pesquisa do Estado de São Paulo (FAPESP, 07/54434-0), Conselho Nacional de Desenvolvimento Científico e Tecnológico (CNPq, 480662/2007-0), and Financiadora de Estudos e Projetos (FINEP, 01.06.0939.00) for financial support, and to the Brazilian Synchrotron Light National Laboratory (LNLS) for assisting the DXAS measurements. Thanks are due to Prof. Peter Hammer (IQ-UNESP) for valuable help in XPS analysis. DRMG thanks FAPESP (Proc. 06/60769-2) and JP thanks CNPq (Proc. 151917/2008-6) for the fellowships granted.

References

[1] C. Lamy, S. Rousseau, E.M. Belgsir, C. Coutanceau, J.-M. Léger, Electrochim. Acta 49 (2004) 3901.
[2] G.A. Camara, T. Iwasita, J. Electroanal. Chem. 578 (2005) 31.
[3] E. Antolini, J. Power Sources 170 (2007) 1.
[4] T. Iwasita, Electrochim. Acta 47 (2002) 3663.
[5] M. Watanabe, S. Motoo, J. Electroanal. Chem. 60 (1975) 267.
[6] N.M. Markovic, H.A. Gasteiger, P.N. Ross, X. Jiang, I. Villegas, M.J. Weaver, Electrochim. Acta 40 (1995) 91.
[7] S.L. Goikovic, T.R. Vidakovic, D.R. Durovic, Electrochim. Acta 48 (2003) 3607.
[8] H.M. Villullas, F.I. Mattos-Costa, L.O.S. Bulhões, J. Phys. Chem. B 108 (2004) 12898.
[9] H.M. Villullas, F.I. Mattos-Costa, P.A.P. Nascente, L.O.S. Bulhões, Chem. Mater. 18 (2006) 5563.
[10] Y. Ishikawa, M.S. Liao, C.R. Cabrera, Surf. Sci. 463 (2000) 66.
[11] P.A. Christensen, A. Hamnett, G.L. Troughton, J. Electroanal. Chem. 362 (1993) 207.
[12] D.R.M. Godoi, J. Perez, H.M. Villullas, J. Phys. Chem. C 113 (2009) 8518.
[13] S. Rousseau, C. Coutanceau, C. Lamy, J.-M. Leger, J. Power Sources 158 (2006) 18.
[14] F. Vigier, C. Coutanceau, A. Perrard, E.M. Belgsir, C. Lamy, J. Appl. Electrochem. 34 (2004) 439.
[15] F. Vigier, C. Coutanceau, F. Hahn, E.M. Belgsir, C. Lamy, J. Electroanal. Chem. 563 (2004) 81.
[16] W. Zhou, Z. Zhou, S. Song, W. Li, G. Sun, P. Tsiakaras, Q. Xin, Appl. Catal. B 46 (2003) 273.
[17] L. Jiang, Z. Zhou, W. Li, W. Zhou, S. Song, H. Li, G. Sun, Q. Xin, Energy Fuels 18 (2004) 866.
[18] L. Jiang, G. Sun, Z. Zhou, W. Zhou, Q. Xin, Catal. Today 93 (2004) 665.
[19] W.J. Zhou, S.Q. Song, W.Z. Li, G.Q. Sun, Q. Xin, S. Kontou, K. Poulianitis, P. Tsiakaras, Solid State Ionics 175 (2004) 797.
[20] F. Colmati, E. Antolini, E.R. González, J. Electrochem. Soc. 154 (2007) B39.
[21] F. Colmati, E. Antolini, E.R. González, Appl. Catal. B: Environ. 73 (2007) 106.
[22] F. Colmati, E. Antolini, E.R. González, J. Solid State Electrochem. 12 (2008) 591.
[23] E.V. Spinacé, M. Linardi, A. Oliveira Neto, Electrochem. Commun. 7 (2005) 365.
[24] Y.X. Bai, J.J. Wu, X.P. Qiu, J.S. Wang, W.T. Zhu, L.Q. Chen, Acta Chim. Sin. 64 (2006) 527.
[25] L. Jiang, G. Sun, S. Sun, J. Liu, S. Tang, H. Li, B. Zhou, Q. Xin, Electrochim. Acta 50 (2005) 5384.
[26] L. Jiang, L. Colmenares, Z. Jusys, G.Q. Sun, R.J. Behm, Electrochim. Acta 53 (2007) 377.
[27] D.R.M. Godoi, J. Perez, H.M. Villullas, J. Electrochem. Soc. 154 (2007) B474.
[28] H.C.N. Tolentino, J.C. Cezar, N. Watanabe, C. Piamonteze, N.M. Souza-Neto, E. Tamura, A. Ramos, R. Neueschwander, Phys. Scr. T115 (2005) 977.
[29] J. McBreen, W.E. O'Grady, K.I. Pandya, R.W. Hoffman, D.E. Sayers, Langmuir 3 (1987) 428.
[30] N.M. Markovic, B.N. Grgur, C.A. Lucas, P.N. Ross, J. Phys. Chem. B 103 (1999) 487.
[31] B. Hayden, M.E. Rendall, O. South, J. Am. Chem. Soc. 125 (2003) 7738.
[32] T.J. Schmidt, H.A. Gasteiger, G.D. Stab, P.M. Urban, D.M. Kolb, R.J. Behm, J. Electrochem. Soc. 145 (1998) 2354.
[33] W.H. Lizcano-Valbuena, V.A. Paganin, C.A.P. Leite, F. Galembeck, E.R. Gonzalez, Electrochim. Acta 48 (2003) 3869.
[34] U.A. Paulus, A. Wokaun, G.G. Scherer, T.J. Schmidt, V. Stamenkovic, N.M. Markovic, P.N. Ross, Electrochim. Acta 47 (2002) 3787.
[35] W.W. Wendlandt, Thermal Analysis, 3rd ed., Wiley, New York, 1986.
[36] J.F. Moulder, J. Chastain, Handbook of X-ray Photoelectron Spectroscopy: A Reference Book of Standard Spectra for Identification and Interpretation of XPS Data, Physical Electronics Division, Perkin-Elmer Corp., Eden Prairie, MN, 1992.
[37] C. Roth, M. Goetz, H. Fuess, J. Appl. Electrochem. 31 (2001) 793.
[38] E. Antolini, L. Giorgi, F. Cardellini, E. Passalacqua, J. Solid State Electrochem. 5 (2001) 131.
[39] J.C. Vedrine, M. Dufaux, C. Naccache, B. Imelik, J. Chem. Soc., Faraday Trans. 1 (74) (1978) 440.
[40] A.K. Shukla, A.S. Arico, K.M. El-Khatib, H. Kim, P.L. Antonucci, V. Antonucci, Appl. Surf. Sci. 137 (1999) 20.
[41] A.K. Shukla, R.K. Raman, N.A. Choudhury, K.R. Priolkar, P.R. Sarode, S. Emura, R. Kumashiro, J. Electroanal. Chem. 563 (2004) 181.
[42] R. Sousa, F. Colmati, E.G. Ciapina, E.R. González, J. Solid State Electrochem. 11 (2007) 1549.
[43] D.W. Marquardt, J. Soc. Ind. Appl. Math. 11 (1963) 431.
[44] M.E. Herron, S.E. Doyle, S. Pizzini, K.J. Roberts, J. Robinson, G. Hards, F.C. Walsh, J. Electroanal. Chem. 324 (1992) 243.
[45] B.J. Hwang, Y.W. Tsai, J.F. Lee, P. Borthen, H.H. Strehblow, J. Synchrotron Radiat. 8 (2001) 484.
[46] S. Mukerjee, J. McBreen, J. Electrochem. Soc. 146 (1999) 600.
[47] X.H. Xia, Electrochim. Acta 45 (1999) 1057.
[48] S. Tillmann, G. Samjeské, K.A. Friedrich, H. Baltruschat, Electrochim. Acta 49 (2003) 73.
[49] H.M. Villullas, F.I. Mattos-Costa, P.A.P. Nascente, L.O.S. Bulhões, Electrochim. Acta 49 (2004) 3909.
[50] M.J. Weaver, S.-C. Chang, L.-W. Leung, X. Jiang, M. Rubel, M. Szklarczyk, D. Zurawski, A. Wieckowski, J. Electroanal. Chem. 327 (1992) 247.
[51] L. Jiang, G. Sun, Z. Zhou, S. Sun, Q. Wang, S. Yan, H. Li, J. Tian, J. Guo, B. Zhou, Q. Xin, J. Phys. Chem. B 109 (2005) 8774.
[52] J. Mann, N. Yao, A.B. Bocarsly, Langmuir 22 (2006) 10432.
[53] M. Zhu, G. Sun, Q. Xin, Electrochim. Acta 54 (2009) 1511.
[54] F. Delime, J.-M. Léger, C. Lamy, J. Appl. Electrochem. 29 (1999) 1249.
[55] C. Lamy, E.M. Belgsir, J.-M. Léger, J. Appl. Electrochem. 31 (2001) 799.
[56] F. Vigier, S. Rousseau, C. Coutanceau, J.-M. Leger, C. Lamy, Top. Catal. 40 (2006) 111.